

# A general solver to the elliptical mixture model through an approximate Wasserstein manifold

Shengxi Li, *Student Member, IEEE*,

Zeyang Yu, Min Xiang, *Member, IEEE*, Danilo Mandic, *Life Fellow, IEEE*

## Abstract

This paper studies the problem of estimation for general finite mixture models, with a particular focus on the elliptical mixture models (EMMs). Instead of using the widely adopted KullbackLeibler divergence, we provide a stable solution to the EMMs that is robust to initialisations and attains superior local optimum by adaptively optimising along a manifold of an approximate Wasserstein distance. More specifically, we first summarise computable and identifiable EMMs, in order to identify the optimisation problem. Due to a probability constraint, solving this problem is cumbersome and unstable, especially under the Wasserstein distance. We thus resort to an efficient optimisation on a statistical manifold defined under an approximate Wasserstein distance, which allows for explicit metrics and operations. This is shown to significantly stabilise and improve the EMM estimations. We also propose an adaptive method to further accelerate the convergence. Experimental results demonstrate excellent performances of the proposed solver.

## I. INTRODUCTION

This paper establishes a general solution to the finite mixture model problem, which has been attracting extensive research effort for decades, due to both its simple representation and potential for universal approximation on arbitrary distributions in  $\mathbb{R}^M$ . The finite mixture model also provides interpretable and statistical descriptions of data, which makes it a popular choice in a wide range of statistical learning paradigms, such as semi-supervised learning [1], capsule networks [2], and various image processing paradigms (e.g., de-noising [3], matching [4] and registration [5]).

The estimation on a finite mixture model boils down to a minimisation problem which considers the mixture of distributions as a parametric model  $\rho(\boldsymbol{\theta})$ , which is then optimised through a minimisation of a certain discrepancy measure between  $\rho(\boldsymbol{\theta})$  and empirical distributions of observed data  $\rho^*$ , namely,  $\min_{\boldsymbol{\theta}} d(\rho(\boldsymbol{\theta}), \rho^*)$ . This minimisation, although not explicitly stated, is a constrained problem because  $\rho(\boldsymbol{\theta})$  must maintain the property of a probability density throughout, to ensure that  $d(\cdot, \cdot)$  is tractable.

Shengxi Li, Zeyang Yu, Min Xiang and Danilo Mandic are with the department of Electrical and Electronic of Imperial College London.

Due to this probability constraint, various advanced numerical algorithms (solvers) are typically restricted by either the requirement of an increasingly flexible  $\rho(\theta)$  or a powerful  $d(\cdot, \cdot)$ . Such restrictions, for example, are one of the main rationales for using the expectation-maximisation (EM) algorithm to minimise the KullbackLeibler (KL) divergence in Gaussian mixture model (GMM) problems [6]. On the other hand, gradient-based numerical algorithms typically rest upon additional techniques that only work in particular situations (e.g., gradient reduction [7], positive definite projection [8], [9], re-parametrisation [10] and Cholesky decomposition [11], [12]). Besides the GMM, there exist other solutions that allow for flexible choices of  $\rho(\theta)$ , which still belong to the EM-type methods (e.g., mixtures of t-distributions [13], [14], [15], Laplace distributions [16] and hyperbolic distributions [17]). Unfortunately, given other suitable candidates of distributions, those EM-type methods cannot ensure universal convergence [18], [19], [20], [21], which dramatically limits the power of finite mixture model in learning various types of data.

Another issue that has been highlighted in the literature is the sensitivity to initialisations when solving GMMs [22], [23]. One of the main reasons is due to the usage of the KL divergence, which operates via a “bin-to-bin” comparison between two density histograms. This means that mixtures which fall into a spurious local minimum cannot be corrected via the points outside. Indeed, with random initialisations for the GMM, Jin has proved that the EM algorithm or other first-order methods minimising the KL divergence are highly likely to result in arbitrary bad local minima [23]. On the other hand, by virtue of the Wasserstein distance<sup>1</sup> [24], [25], [26] which employs a “cross-bin” comparison, many practical benefits may be achieved in learning tasks [27], [28], [29] due to the reflection of sample space [30]. This property is particularly appealing in mixture model problems, where it ideally provides a comprehensive distance measure over all possible transport plans, and promises to achieve superior optimisation. Most recently, Kolouri *et al.* [31] have adopted the Wasserstein distance for solving GMM problems. However, the aforementioned probability constraint enforces an extremely small stepsize (learning rate) during optimisation. Given the random projections of the sliced Wasserstein distance, this setup leads to extremely slow convergence or even non-convergence. At the end of the optimisation, in their provided code, the EM algorithm is still needed to stabilise the optimisation.

**Motivations and Contributions:** Despite extensive benefits, optimising the GMM under the Wasserstein distance is still not feasible due to the probability constraint. To address this constraint from a different perspective, we resort to the statistical manifold. We should further point out that our work is different from information geometry [32], [33], as directly establishing the manifold in the whole density space of mixture models is absolutely intractable and cumbersome in optimisation [34], [35], [36]. Another problem within the Wasserstein space is that the geodesic between two mixture models may not lie in mixture models of the same type [37], which leads to non-convergence.

<sup>1</sup>Throughout this paper, the Wasserstein distance refers to the square-Wasserstein distance.

We propose to resolve this problem by introducing an approximation to the Wasserstein distance and then proceed to establish the statistical manifold via the so induced distance, which is complete within mixture models. The subsequent optimisation along this manifold intrinsically satisfies the probability constraint and ensures that the solution resides in the same mixture models. More importantly, minimising the induced distance is shown to be truly reducing the discrepancy of two mixture models, unlike most existing research which is based on the minimisation of the Euclidean distance from the optimal parameters. This ensures fast and stable convergence in optimisation. By realising that the existing Riemannian adaptive algorithms only make sense in updating vector parameters, we further develop a novel accelerated stochastic gradient descent method for updating the positive definite matrices.

In this way, our proposed framework makes it possible to incorporate a broad family of distributions  $\rho(\theta)$ , including an important class of multivariate analysis techniques called elliptical distributions [38] and to investigate the mixture family termed the elliptical mixture model (EMM). We therefore provide the computable and identifiable EMMs with a unified framework, which shows that EMMs are quite general and flexible and include the GMMs as special cases [38].

Therefore, this paper proposes a complete and efficient framework for general EMM problems, by establishing a statistical manifold under an approximate Wasserstein distance which promotes stability and efficiency, and through an adaptive stochastic gradient algorithm to further accelerate the optimisation. Compared to the existing literature on mixture problems, the proposed solution achieves consistently superior performance not only in the GMM problems but also for general EMM problems. Our contributions can be summarised as follows,

- A unified framework for dealing with computable and identifiable EMMs, which introduces a rich candidates for flexible finite mixture models.
- Establishment of the statistical manifold through the proposed approximate Wasserstein distance, which provides explicit and complete operations within the manifold.
- Adaptively accelerated Riemannian gradient descent algorithm on the established manifold, to improve the optimisation and accelerate convergence.

## II. COMPUTABLE AND IDENTIFIABLE EMMs

Elliptical distributions include a wide range of standard distributions, and it therefore comes as no surprise that a unified summary of computable candidates as components in the EMMs is a prerequisite to problem definition and subsequent solutions. A classical summary can be found in Chapter 3 in [38], however, various elliptical distributions in the recent decade are missing, and more importantly, it involves complicated representations for each type of elliptical distributions. The existing literature also employs different notations and formulations of particular distributions, which may lead to confusion. To this end, we provide a simple and unified framework for summarising the existing computable elliptical distributions via the stochastic representation, which can then be used to constitute flexible and identifiable EMMs.

### A. Preliminaries on elliptical distributions

A random variable  $\mathcal{X} \in \mathbb{R}^m$  is said to have an elliptical distribution if and only if it admits the following stochastic representation [39],

$$\mathcal{X} \stackrel{d}{=} \boldsymbol{\mu} + \mathcal{R}\boldsymbol{\Lambda}\boldsymbol{S}, \quad (1)$$

where  $\mathcal{R} \in \mathbb{R}^+$  is a non-negative real scalar random variable which models tail properties of the elliptical distribution;  $\boldsymbol{S} \in \mathbb{S}^{(m'-1)}$  is a random vector that is uniformly distributed on a unit spherical surface<sup>2</sup> with the pdf within the class of  $2\pi^{-m'/2}\Gamma(m'/2)$ ;  $\boldsymbol{\mu} \in \mathbb{R}^m$  is a mean (location) vector, while  $\boldsymbol{\Lambda} \in \mathbb{R}^{m \times m'}$  is a matrix that transforms  $\boldsymbol{S}$  from a sphere to an ellipse, and “ $\stackrel{d}{=}$ ” designates “the same distribution”. For a comprehensive review of elliptical distributions, we refer to [38], [40].

When  $m' = m$ , that is, for a non-singular scatter matrix  $\boldsymbol{\Sigma} = \boldsymbol{\Lambda}\boldsymbol{\Lambda}^T$ , the pdf for elliptical distributions does exist and has the following form

$$p(\mathbf{x}) = \underbrace{2\pi^{-m/2}\Gamma(m/2)}_{c_m} \det(\boldsymbol{\Sigma})^{-1/2} g(\underbrace{(\mathbf{x} - \boldsymbol{\mu})^T \boldsymbol{\Sigma}^{-1} (\mathbf{x} - \boldsymbol{\mu})}_t). \quad (2)$$

In (2), the term  $c_m$  serves as a normalisation term and solely relates to  $m$ . We denote the Mahalanobis distance  $(\mathbf{x} - \boldsymbol{\mu})^T \boldsymbol{\Sigma}^{-1} (\mathbf{x} - \boldsymbol{\mu})$  by  $t$ . The density generator,  $g(t)$ , can be explicitly expressed as  $t^{-(m-1)/2} p_{\mathcal{R}}(\sqrt{t})$ , where  $t > 0$  and  $p_{\mathcal{R}}(t)$  denotes the pdf of  $\mathcal{R}$ . Thus,  $\mathcal{R}$ , or equivalently<sup>3</sup>  $\mathcal{R}^2$ , fully characterises  $g(\cdot)$ , i.e., the type of elliptical distributions. For example, when  $\mathcal{R}^2 \stackrel{d}{=} \chi_m^2$  ( $\chi_m^2$  denotes the chi-squared distribution of dimension  $m$ ), then in (2),  $g(t) \propto \exp(-t/2)$ , which formulates the multivariate Gaussian distribution. Therefore, the elliptical distribution can be fully characterised by  $\boldsymbol{\mu}$ ,  $\boldsymbol{\Sigma}$  and  $\mathcal{R}$ . For simplicity, the elliptical distribution in (2) will be denoted by  $\mathcal{X} \sim \mathcal{E}(\mathbf{x}; \boldsymbol{\mu}, \boldsymbol{\Sigma}, \mathcal{R})$ , where  $\mathcal{E}(\mathbf{x}; \boldsymbol{\mu}, \boldsymbol{\Sigma}, \mathcal{R}) = c_m \det(\boldsymbol{\Sigma})^{-1/2} g(t)$  of (2).

### B. Computable and identifiable EMMs

Due to the fact that the  $\mathcal{R}^2$  decides the type of elliptical distributions, we here provide a unified summary of elliptical distributions in Table I; this is achieved through stochastic representations in (1). This makes it possible to avoid complicated formulations, and to instead classify different categories simply through several typical distributions of  $\mathcal{R}^2$ , which also allows for simple and intuitive sample generations for elliptical distributions. The proof for expressions in this table is provided in the Appendix-A. Uniquely, this further clarifies the commonalities between the members of the elliptical family of distributions. More importantly, constructing an EMM with the candidates in Table I can be easily proved to be identifiable based on Theorem 2 in [41]. It is thus convenient and safe to establish a well-defined EMM by the candidates summarised in Table I.

<sup>2</sup> $\mathbb{S}^{m'-1}$  is defined as  $\mathbb{S}^{m'-1} := \{\mathbf{x} \in \mathbb{R}^{m'} : \mathbf{x}^T \mathbf{x} = 1\}$ .

<sup>3</sup>The term  $\mathcal{R}^2$  is frequently used in practice because  $\mathcal{R}^2 \stackrel{d}{=} (\mathbf{x} - \boldsymbol{\mu})^T \boldsymbol{\Sigma}^{-1} (\mathbf{x} - \boldsymbol{\mu})$ .

TABLE I  
 $\mathcal{R}^2 \leftrightarrow$  COMPUTABLE ELLIPTICAL DISTRIBUTIONS

Types	$\mathcal{R}^2$	$\leftrightarrow$	$c_m \cdot g(t)$	Typical Multivariate Dist.
<b>Kotz Type [38]</b>	$\mathcal{R}^2 = {}^d \mathcal{G}^{1/s},$ $\mathcal{G} \sim \text{Ga}(\frac{2a+m-2}{2s}, b),$ $a > 1 - \frac{m}{2}, b, s > 0$	$\leftrightarrow$	$= \left( \frac{\Gamma(m/2) s b^{(2a+m-2)/(2s)}}{\Gamma((2a+m-2)/2s) \pi^{m/2}} \right) t^{a-1} \exp(-bt^s)$	Gamma: $s = 1$ Weibull: $a = s$ Generalised Gaussian: $a = 1$ Gaussian: $a = 1, s = 1, b = \frac{1}{2}$
<b>Scale Mixture of Normals</b>	Pearson Type VII [38] $\mathcal{K}^{-1} \sim \text{Ga}(s - \frac{m}{2}, 2v),$ $v > 0, s > m/2$	$\leftrightarrow$	$= \left( \frac{(\pi v)^{-m/2} \Gamma(s)}{\Gamma(s - m/2)} \right) (1 + t/v)^{-s}$	T-dist.: $s = \frac{m+v}{2}$ Cauchy: $v = 1, s = \frac{m+1}{2}$
$\mathcal{R}^2 = {}^d \mathcal{G} \cdot \mathcal{K},$ $\mathcal{G} \sim \text{Ga}(\frac{m}{2}, \frac{1}{2}), \mathcal{K}$ has different dist.	Hyperbolic Type [42], [17] $\mathcal{K} \sim \text{GIG}(v, a, \lambda)$ $v, a > 0, \lambda \in \mathbb{R}$	$\leftrightarrow$	$= \left( \frac{(v/a)^{\lambda/2}}{(2\pi)^{m/2} \text{BeK}_\lambda(\sqrt{av})} \right) \frac{\text{BeK}(\lambda - m/2)(\sqrt{av+vt})}{(\sqrt{a/v+tv})^{m/2-\lambda}}$	Inverse-Gaussian: $\lambda = -1/2$ K-dist. [43]: $a \rightarrow 0, \lambda > 0$ Laplace: $a \rightarrow 0, \lambda = 1, v = 2$
	Other Types [21], [44] $\sqrt{\mathcal{K}} \sim \partial \text{Kov}(\frac{\mathcal{K}}{2}) / \partial \mathcal{K}$	$\leftrightarrow$	$= \exp(-t) / (1 + \exp(-t))^2$	Logistic
	$\mathcal{K} \sim \text{SaS}(\frac{a}{2}), a \in (0, 2)$	$\leftrightarrow$	$\propto \text{SaS}(a)$	$\alpha$ -stable
<b>Pearson Type II [38]</b>	$\mathcal{R}^2 \sim \text{Beta}(m/2, s), s > 1$	$\leftrightarrow$	$= \left( \frac{\Gamma(m/2+s)}{\pi^{m/2} \Gamma(s)} \right) (1-t)^{s-1}, t \in [0, 1]$	-
Notations:	$a, b, s, v, \lambda, \alpha$ are adjustable parameters for different types of dist.; $\mathcal{G}$ and $\mathcal{K}$ are random variables related to $\mathcal{R}^2$ ; $m$ is the dimension. Gamma dist.: $\text{Ga}(x, y) = y^x t^{x-1} \exp(-yt) / \Gamma(x)$ ; Inverse Gaussian dist.: $\text{GIG}(x, y, z) = \frac{(x/y)^{z/2}}{2 \text{BeK}_z(\sqrt{xy})} t^{z-1} \exp(-\frac{xt^2+y}{2t})$ ; Kolmogorov-Smirnov dist.: $\text{Kov}(x) = 1 - 2 \sum_{n=1}^{\infty} (-1)^{n+1} \exp(-2n^2 x^2)$ ; Beta dist.: $\frac{\Gamma(x+y)}{\Gamma(x)\Gamma(y)} t^{x-1} (1-t)^{y-1}$ ; $\text{SaS}(a)$ : the symmetric $\alpha$ -stable dist. with index $a$ ; $\text{BeK}_x(y)$ : the Bessel function of the third kind; $\Gamma(x)$ : the Gamma function.			

### C. Problem statement and notations

Generally we assume that there are  $k$  mixtures in the EMM model, latent variables  $\mathcal{Z}_i \in \{0, 1\}$  are binary, and the probability of choosing the  $i$ -th mixture is denoted by  $p(\mathcal{Z}_i = 1) = \pi_i$ , so that  $\sum_{i=1}^k \mathcal{Z}_i = 1$  and  $\sum_{i=1}^k \pi_i = 1$ . If we use the random variable  $\mathcal{Y}$  to denote the EMM, then  $\mathcal{Y} = {}^d \sum_{i=1}^k \mathcal{Z}_i \mathcal{X}_i \sim \sum_{i=1}^k \pi_i \mathcal{E}(\mathbf{x} | \boldsymbol{\mu}_i, \boldsymbol{\Sigma}_i, \mathcal{R})$ , and the pdf of  $\mathcal{Y}$  can be expressed as

$$p(\mathbf{y}) = \sum_{i=1}^k \pi_i c_m \det(\boldsymbol{\Sigma}_i)^{-1/2} g((\mathbf{y} - \boldsymbol{\mu}_i)^T \boldsymbol{\Sigma}_i^{-1} (\mathbf{y} - \boldsymbol{\mu}_i)), \quad (3)$$

where the density generator  $g(\cdot)$  can be flexibly chosen from Table I, for which the identifiability is ensured [41]. Thus, without ambiguity in the context, we also denote the EMM  $\mathcal{Y}$  with the pdf of (3) as  $\mathcal{Y}_\theta$ , where  $\theta = \{\boldsymbol{\pi}, \boldsymbol{\mu}_i, \boldsymbol{\Sigma}_i\}$  ( $\boldsymbol{\pi} = [\pi_1, \pi_2, \dots, \pi_k]^T$  and  $i = 1, 2, \dots, k$ ).

### III. STATISTICAL MANIFOLD TOWARDS EMMs

As the Wasserstein distance possesses a Riemannian structure [45], [30], it is thus natural to treat each EMM as a “point” in the manifold, whereby the metric is defined by the Hessian of the Wasserstein distance. However, as pointed out by Chen [37], in the Wasserstein space, the geodesic between two points, i.e., two GMMs, does not necessarily belong to the GMM of the same type. A way to solve this problem is to pull back from the whole density space to the parametric space [37]. This treatment, nevertheless, is still a toy solution due to two main considerations. The first deficiency is that the metric does not have a closed-form representation, which needs to be numerically obtained for every possible value in advance before the optimisation. This is highly prohibitive, especially for multivariate cases due to the curse of dimensionality. Besides computational intractability, operations such as the exponential mapping and the vector transport in the manifold cannot be well defined as there is typically a second-order differential equation involved to obtain those operations [46].

We thus propose an approximate Wasserstein distance between two EMMs as a means to define a well-behaved manifold for the EMM problems; this is achieved by the property that the Wasserstein distance of two elliptical distributions is completely and explicitly defined. We then provide the Riemannian metric for the EMM problems according to the defined distance.

#### A. An approximate Wasserstein distance between two EMMs

We now focus on the distance between two EMMs  $\mathcal{Y}_1$  and  $\mathcal{Y}_2$ , and propose an approximate Wasserstein distance by treating each distribution within an EMM as a “super-point” and defining a transport-like distance between those “super-points”. A rigorous definition is given as follows.

**Definition 1.** Given two EMMs  $\mathcal{Y}_1$  and  $\mathcal{Y}_2$ , a discrepancy measure is defined as

$$d_U(\mathcal{Y}_1, \mathcal{Y}_2) = \min_{\gamma(i,j)} \left( \sum_{i,j} \frac{\gamma(i,j)}{k} d_W^2(\mathcal{X}_{i,1}, \mathcal{X}_{j,2}) + \arccos\left(\sum_{i,j} \gamma(i,j) \sqrt{\pi_{i,1}\pi_{j,2}}\right) \right), \quad (4)$$

where  $d_W^2(\mathcal{X}_{i,1}, \mathcal{X}_{j,2})$  is the Wasserstein distance between the elliptical distributions  $\mathcal{X}_{i,1}$  and  $\mathcal{X}_{j,2}$ .  $\gamma(i, j)$  is binary  $\in \{0, 1\}$ ; for each  $i$  and  $j$ ,  $\gamma(i, j)$  satisfies  $\sum_{i=1}^k \gamma(i, j) = 1$  and  $\sum_{j=1}^k \gamma(i, j) = 1$ .

**Theorem 1.** Given two EMMs  $\mathcal{Y}_1$  and  $\mathcal{Y}_2$ ,  $d_U(\mathcal{Y}_1, \mathcal{Y}_2)$  defines a distance.

*Proof.* Please refer to the Appendix-B for a complete proof. □

By definition,  $\arccos(\sum_{i,j} \gamma(i, j) \sqrt{\pi_{i,1}\pi_{j,2}})$  intrinsically involves the probability constraint of  $\sum_{i=1}^k \pi_{i,1} = \sum_{j=1}^k \pi_{j,2} = 1$ , while  $\gamma(i, j)$  operates as a bijection between mixture components in  $\mathcal{Y}_1$  and  $\mathcal{Y}_2$ .  $\sum_{i,j} \frac{\gamma(i,j)}{k} d_W^2(\mathcal{X}_{i,1}, \mathcal{X}_{j,2})$  can thus be regarded as a discrete transport between  $k$  uniformly distributed “super-points”  $\mathcal{X}_{i,1}$  and  $\mathcal{X}_{j,2}$ , for which their cost is defined as  $d_W^2(\mathcal{X}_{i,1}, \mathcal{X}_{j,2})$ .

More importantly,  $d_U(\mathcal{Y}_1, \mathcal{Y}_2)$  comprehensively reflects the discrepancy between  $\mathcal{Y}_1$  and  $\mathcal{Y}_2$  because either the difference between mixture components  $\mathcal{X}_{i,1}$  and  $\mathcal{X}_{j,2}$  or the difference between latent variables  $\pi_{i,1}$  and  $\pi_{j,2}$  can be well reflected. The following lemma further proves that for balanced EMMs,  $d_U(\mathcal{Y}_1, \mathcal{Y}_2)$  is an upper bound of the Wasserstein distance  $d_W^2(\mathcal{Y}_1, \mathcal{Y}_2)$ .

**Lemma 1.** *Given two balanced EMMs  $\mathcal{Y}_1$  and  $\mathcal{Y}_2$  (i.e.,  $\pi_{i,1} = \pi_{j,2} = 1/k$  for all  $i, j$ ),  $d_U(\mathcal{Y}_1, \mathcal{Y}_2)$  is an upper bound of the Wasserstein distance:*

$$d_W^2(\mathcal{Y}_1, \mathcal{Y}_2) \leq d_U(\mathcal{Y}_1, \mathcal{Y}_2). \quad (5)$$

The equality holds when  $k = 1$ .

*Proof.* Please refer to the Appendix-C. □

### B. Statistical manifold for EMM problems

Before we introduce the statistical manifold for EMMs, we need to credit several most recent works towards Gaussian distributions and elliptical distributions, which lay a basis of our metric developed in this section. We would like to mention [47], [48], [48], [49] for the Wasserstein distance of Gaussian measures and [50], [51] for the elliptical distributions. Most recently, the Riemannian manifold for Gaussian distributions has been established in an explicit form [52], [53]. Then, on the basis of the approximated Wasserstein distance, we provide the Riemannian metric of the EMM problems by calculating the Hessian of the proposed distance in Definition 1 as follows.

**Lemma 2.** *The approximate Wasserstein distance  $d_U(\mathcal{Y}_1, \mathcal{Y}_2)$  possesses an explicit Riemannian metric in the parametric space, and the corresponding Riemannian manifold is a product manifold of  $\mathbb{R}^k \times \prod_{i=1}^k (\mathbb{R}^m \times \mathbb{P})$ , where  $\mathbb{P}$  is the  $m \times m$  positive definite manifold:*

- 1) *The manifold for the square root of  $\pi_i$ , i.e.,  $[\sqrt{\pi_1}, \sqrt{\pi_2}, \dots, \sqrt{\pi_k}]^T$  is a sphere manifold of  $\mathbb{R}^k$ .*
- 2) *The manifold for  $\mu_i$  is the plain Euclidean space of  $\mathbb{R}^m$ .*
- 3) *The manifold for  $\Sigma_i$ , i.e.,  $\mathbb{P}$ , is defined by*

$$ds^2 = \frac{\mathbb{E}[\mathcal{R}^2]}{m} (\mathbb{L}_{\Sigma_i}[d\Sigma]) \Sigma_i (\mathbb{L}_{\Sigma_i}[d\Sigma]). \quad (6)$$

In (6),  $\mathbb{L}_A[\mathbf{C}] = \mathbf{B}$  is a Lyapunov operator:  $\mathbf{A}\mathbf{B} + \mathbf{B}\mathbf{A} = \mathbf{C}$ , where  $\mathbf{A}, \mathbf{B}, \mathbf{C} \in \mathbb{P}$ . More importantly, the sectional curvature is non-negative ( $= m/\mathbb{E}[\mathcal{R}^2]k_G$  where  $k_G \geq 0$  is the sectional curvature for Gaussian cases [52]). Recall that  $\mathcal{R}$  is defined in the stochastic representation of (1).

*Proof.* Please refer to the Appendix-D. □

**Remark.** *The metric in (6) provides a manifold for positive definite matrices. Compared to the most well-known manifold belonging to the Hadamard manifold (non-positive sectional curvature) [54], the newly developed*

manifold provides an example of non-negative manifolds. It is actually further stated that an Alexandrov space has the non-negative curvature iff it is a Wasserstein space [55].

#### IV. ADAPTIVELY ACCELERATED OPTIMISATION IN SOLVING EMMs

Given the idea of optimising on the statistical manifold, the probability constraint can be satisfied automatically, which allows us to incorporate various numerical algorithms in solving the EMM problems. Specifically, we first show that the constrained minimisation problem can be transformed to an unconstrained one when restricted in the statistical manifold, which results in the vanilla gradient descent on the manifold. Then, we further propose an adaptively accelerated algorithm.

##### A. Vanilla gradient descent on the statistical manifold of EMMs

Similar to [33], for the gradient descent methods, the way for descending in our work is as follows.

$$\Delta\theta^* = \arg \min_{\Delta\theta \text{ s.t. } d_U(\mathcal{Y}_\theta, \mathcal{Y}_{\theta+\Delta\theta}) \leq c^2} d_{SW}(\mathcal{Y}_{\theta+\Delta\theta}, \mathcal{Y}^*) \rightarrow \Delta\theta^* = \text{Exp}(-\alpha \nabla_U(\theta)), \quad (7)$$

where  $\Delta\theta$  is the step size for the next iteration and  $c^2$  denotes a sphere of all realisable distributions, which ensures searching for optimal  $\Delta\theta^*$  without being slowed down by the curvature;  $d_{SW}(\mathcal{Y}_{\theta+\Delta\theta}, \mathcal{Y}^*)$  denotes the sliced Wasserstein distance [56] between the parametric mixture model  $\mathcal{Y}_{\theta+\Delta\theta}$  and the observed samples  $\mathcal{Y}^*$ . By approximating  $d_U(\mathcal{Y}_\theta, \mathcal{Y}_{\theta+\Delta\theta})$  with its Hessian term (i.e., the inner product on the tangent space), we naturally obtain an unconstrained Riemannian gradient descent of the right side of (7), where  $\nabla_U(\theta)$  is the Riemannian gradient on the statistical manifold defined by  $d_U(\cdot, \cdot)$ ;  $\alpha$  is the stepsize of each iteration;  $\text{Exp}(-\alpha \nabla_U(\theta))$ , called exponential mapping, projects the step movement  $-\alpha \nabla_U(\theta)$  from the tangent space to the statistical manifold along geodesics [57], which ensures the probability constraint. On the other hand, when the proposed distance  $d_U(\mathcal{Y}_\theta, \mathcal{Y}_{\theta+\Delta\theta})$  is changed to the Euclidean distance, (7) is the trivial gradient descent [31], [33]. However, as aforementioned, this gradient descent does not satisfy the probability constraint or reflect the probability space curvature, which leads to inefficient and unstable optimisation.

In (7), the sliced Wasserstein distance [56] provides a feasible solution in solving the semi-discrete Wasserstein problem, i.e.,  $\mathcal{Y}_{\theta+\Delta\theta}$  is continuous and  $\mathcal{Y}^*$  is the sum of Dirac masses [58]. It uses unit random projections to turn the original problem to an one-dimensional Wasserstein problem via the Radon transform [56], whereby a closed-form solution can be obtained. More importantly, as the sliced Wasserstein distance is composed of a set of random projections [56], it is thus natural to implement a stochastic gradient descent on the Riemannian manifold for each random projection (denoted as  $\mathbf{p} \in \mathbb{S}^{m-1}$ ). The random projection process also allows a parallel gradient descent. We thus provide the basic operations of problem (7) in Table II, in which the detailed calculation under the sliced Wasserstein distance is proved in the Appendix-E.



TABLE II  
BASIC OPERATIONS OF THE MANIFOLD IN LEMMA 2

For the $h$ -th iteration		
	$\nabla_U(\cdot)$	$\text{Exp}(-\alpha \nabla_U(\cdot))$
$\sqrt{\boldsymbol{\pi}}^h$	$\nabla_E(\sqrt{\boldsymbol{\pi}}^h) - (\sqrt{\boldsymbol{\pi}}^h)^T \nabla_E(\sqrt{\boldsymbol{\pi}}^h) \cdot \sqrt{\boldsymbol{\pi}}^h$	$\cos(\ \alpha \nabla_U(\sqrt{\boldsymbol{\pi}}^h)\ _2) \sqrt{\boldsymbol{\pi}}^h - \frac{\sin(\ \alpha \nabla_U(\sqrt{\boldsymbol{\pi}}^h)\ _2)}{\ \nabla_U(\sqrt{\boldsymbol{\pi}}^h)\ _2} \nabla_U(\sqrt{\boldsymbol{\pi}}^h)$
$\boldsymbol{\mu}_i^h$	$\nabla_E(\boldsymbol{\mu}_i^h)$	$\boldsymbol{\mu}_i^h - \alpha \nabla_U(\boldsymbol{\mu}_i^h)$
$\boldsymbol{\Sigma}_i^h$	$\nabla_E(\boldsymbol{\Sigma}_i^h) \boldsymbol{\Sigma}_i^h + \boldsymbol{\Sigma}_i^h \nabla_E(\boldsymbol{\Sigma}_i^h)$	$(\mathbb{L}_{\boldsymbol{\Sigma}_i^h}[-\alpha \nabla_U(\boldsymbol{\Sigma}_i^h)] + I) \boldsymbol{\Sigma}_i^h (\mathbb{L}_{\boldsymbol{\Sigma}_i^h}[-\alpha \nabla_U(\boldsymbol{\Sigma}_i^h)] + I)$
For the Radon transform $\mathbf{p} \in \mathbb{S}^{m-1}$ , specified in the EMM problems:		
$\nabla_E(\sqrt{\boldsymbol{\pi}}^h)$	The $i$ -th dimension of $\nabla_E(\sqrt{\boldsymbol{\pi}}^h)$ is $2 \int_{\mathbb{R}} c_m \phi(y) \sqrt{\pi_i^h} (\mathbf{p}^T \boldsymbol{\Sigma}_i^h \mathbf{p})^{-1/2} g\left(\frac{(y - \mathbf{p}^T \boldsymbol{\mu}_i^h)^2}{\mathbf{p}^T \boldsymbol{\Sigma}_i^h \mathbf{p}}\right) dy$	
$\nabla_E(\boldsymbol{\mu}_i^h)$	$= \left( -2 \int_{\mathbb{R}} c_m \phi(y) \pi_i^h (\mathbf{p}^T \boldsymbol{\Sigma}_i^h \mathbf{p})^{-3/2} g'\left(\frac{(y - \mathbf{p}^T \boldsymbol{\mu}_i^h)^2}{\mathbf{p}^T \boldsymbol{\Sigma}_i^h \mathbf{p}}\right) (y - \mathbf{p}^T \boldsymbol{\mu}_i^h) dy \right) \mathbf{p}$	
$\nabla_E(\boldsymbol{\Sigma}_i^h)$	$= \left( - \int_{\mathbb{R}} c_m \phi(y) \pi_i^h (\mathbf{p}^T \boldsymbol{\Sigma}_i^h \mathbf{p})^{-3/2} \left( \frac{1}{2} g\left(\frac{(y - \mathbf{p}^T \boldsymbol{\mu}_i^h)^2}{\mathbf{p}^T \boldsymbol{\Sigma}_i^h \mathbf{p}}\right) + g'\left(\frac{(y - \mathbf{p}^T \boldsymbol{\mu}_i^h)^2}{\mathbf{p}^T \boldsymbol{\Sigma}_i^h \mathbf{p}}\right) \frac{(y - \mathbf{p}^T \boldsymbol{\mu}_i^h)^2}{\mathbf{p}^T \boldsymbol{\Sigma}_i^h \mathbf{p}} \right) dy \right) \mathbf{p} \mathbf{p}^T$	
$\phi(y)$ is the Kantorovich potential [37]. $\nabla_E(\cdot)$ denotes the Euclidean gradient with regard to $\sqrt{\boldsymbol{\pi}}^h$ , $\boldsymbol{\mu}_i^h$ and $\boldsymbol{\Sigma}_i^h$ .		

### B. Adaptively accelerated Riemannian stochastic gradient descent

On the basis of several accelerated Riemannian stochastic gradient descent methods by adopting the first-order moment information [59], [60], [61], [62], [63], most recently, Becigneu and Ganea [64] further proposed a Riemannian adaptive method by employing the second-order moments. Although this adaptive stochastic gradient descent method [64] can be incorporated to further improve the convergence performance in our work, we argue that it only makes sense for updating vector parameters, i.e.,  $\boldsymbol{\pi}^h$  and  $\boldsymbol{\mu}_i^h$ , because in this case the second-order moment can be element-wisely calculated by decomposition into product manifolds [64]. This is similar to the *Adam* algorithm in the Euclidean space [65]. When updating the matrix parameter  $\boldsymbol{\Sigma}_i^h$ , however, it does not capture the second-order information properly due to the direct accumulation of the second-order moments over the whole matrix manifold, which slows down the convergence in optimisation.

The key difficulty for the matrix case is that it is meaningless to accumulate second-order moments in an element-wise manner due to the structures within the matrix. We view the second-order moments of matrices from another perspective, by realising that a positive definite matrix can be decomposed into a set of eigenvectors and the corresponding eigenvalues. The eigenvectors can be regarded as a set of projection directions and the eigenvalues are scalars that can be connected with the accumulation in those directions. Furthermore, we can find from Table II that the Euclidean gradient  $\nabla_E(\boldsymbol{\Sigma}_i^h)$  consists of a scalar weight multiplied by a rank-1 matrix characterised by

---

**Algorithm 1:** Riemannian adaptively accelerated manifold optimisation

---

**Input:**  $n$  observed samples  $\mathbf{y}_1, \mathbf{y}_2, \dots, \mathbf{y}_n$ ; stepsize  $\{\alpha^h\}_{h=1}^H$ ; hyper-parameters  $\{\beta_1^h\}_{h=1}^H$  and  $\beta_2$

**Initialise:** first-order moment  $\{\mathbf{u}_i^0\}_{i=1}^k = \mathbf{0}$ ; second-order moment  $\{\mathbf{v}_i^0\}_{i=1}^k = \mathbf{0}$

**for:**  $h = 1$  to  $H$  **do**

Random projection:  $\mathbf{p} \in \mathbb{S}^{(m-1)}$

Update  $\sqrt{\boldsymbol{\pi}}^{h+1} = \text{Exp}(-\alpha \nabla_U(\sqrt{\boldsymbol{\pi}}^h))$

**for:**  $i = 1$  to  $k$  **do**

Update  $\boldsymbol{\mu}_i^{h+1} = \text{Exp}(-\alpha \nabla_U(\boldsymbol{\mu}_i^h))$

Update  $\boldsymbol{\Sigma}_i^h$  by the *Dadam*:

$$\mathbf{u}_i^h = \beta_1^h \varphi_{\boldsymbol{\Sigma}_i^{h-1} \rightarrow \boldsymbol{\Sigma}_i^h}(\mathbf{u}_i^{h-1}) + (1 - \beta_1^h) \nabla_U(\boldsymbol{\Sigma}_i^h)$$

$$\mathbf{v}_i^h = \beta_2 \mathbf{v}_i^{h-1} + (1 - \beta_2) \nabla_E(\boldsymbol{\Sigma}_i^h) \nabla_E(\boldsymbol{\Sigma}_i^h)^T$$

$$\text{adp}_i^h = \max\{\mathbf{p}^T \mathbf{v}_i^h \mathbf{p}, \text{adp}_i^{h-1}\}$$

$$\boldsymbol{\Sigma}_i^{h+1} = \text{Exp}(-\alpha^h \mathbf{u}_i^h / \sqrt{\text{adp}_i^h})$$

**end for**

**end for**

**Return:**  $\boldsymbol{\pi}^H, \{\boldsymbol{\mu}_i^H\}_{i=1}^k, \{\boldsymbol{\Sigma}_i^H\}_{i=1}^k$

---

the direction  $\mathbf{p}\mathbf{p}^T$ . Therefore, instead of the element-wise accumulation, we propose a direction-wise accumulation of second-order moments to adaptively adjust the stepsize when updating the matrix. We provide the details of our algorithm in Algorithm 1, in which our directional adaptive accelerated method (*Dadam*) of updating  $\boldsymbol{\Sigma}_i^h$  is achieved by  $\mathbf{v}_i^h$  and  $\text{adp}_i^h$ . It needs to be pointed out that  $\text{adp}_i^h$  denotes the accumulation in the current projection  $\mathbf{p}$ , which is a scalar for computational ease instead of computing an inverse of  $\mathbf{v}_i^h$ . This also makes our convergence analysis similar to that of [64], by realising that the sectional curvature is automatically bounded from below. We thus omit the analysis here. Moreover, as there is no explicit parallel transport in the Wasserstein space, we propose a new vector transport way  $\varphi_{\boldsymbol{\Sigma}_i^{h-1} \rightarrow \boldsymbol{\Sigma}_i^h}(\mathbf{u}_i^{h-1}) = \mathbb{L}_{\boldsymbol{\Sigma}_i^{h-1}}[\mathbf{u}_i^{h-1}] \boldsymbol{\Sigma}_i^h + \boldsymbol{\Sigma}_i^h \mathbb{L}_{\boldsymbol{\Sigma}_i^{h-1}}[\mathbf{u}_i^{h-1}]$  to accumulate the first-order moments.

## V. EXPERIMENTAL RESULTS

In this section, we evaluate the effectiveness of our established manifold and the proposed *Dadam* on both synthetic data and image data, by employing 4 EMMs, i.e., mixtures of *Gaussian*, *Logistic*, *Cauchy* and *Gamma*

( $s = 1, a = 2, b = 0.5$  in Table I).

**Synthetic data:** Each synthetic dataset contains different mixtures of Gaussian distributions, with 10,000 samples in total. Specifically, we employed three types of synthetic datasets, i.e.,  $\{m = 2, k = 3\}$ ,  $\{m = 8, k = 9\}$  and  $\{m = 16, k = 27\}$ . Each type contains 10 randomly generated mixture datasets (eccentricity  $\varepsilon$  of [66] and separation  $c$  of [66] were equal to 10). For every dataset, we tested each algorithm for 10 random initialisations and recorded the mean and standard deviation.

**Image data:** The whole BSDS500 [67] benchmark dataset for image segmentation was employed in our evaluation, which contains 500 images in total. Each image was tested with 10 random initialisations, where the mean and standard deviation were recorded.

**Parameter settings and metrics:** We found the best learning rates  $\alpha$  by searching from  $\{0.001, 0.003, 0.01, 0.03, 0.1, 0.3\}$ . Similar to [65], [64],  $\beta_{11} = 0.9$  and  $\beta_2 = 0.999$ . The maximum number of iterations for testing the synthesis data was 2,000 and that for the image data is 5,000. The Wasserstein distance (simplified as *Wass*) and averaged negative log-likelihood (*NLL*) were mainly employed for comparison. The optimisation fail ratio (*FailR*) was also reported to show the stability of optimisation under various initialisations. For image data, we also adopted two well-known metrics, i.e., the peak signal-to-noise ratio (*PSNR*) and structural similarity index (*SSIM*) [68] to evaluate the quality of reconstructed images via maximising the posterior of optimised EMMs.

**Baselines:** Each main part of our algorithm was assessed. We denote the vanilla Riemannian gradient descent method on our manifold as *W/M + Vanilla*. The Riemannian *Adam* of [64] with our manifold is *W/M + Adam*. Our proposed *Dadam* is denoted as *W/M + DAdam*. On the other hand, we compared with the trivial gradient descent method over the sliced Wasserstein distance without the manifold (denoted by *WO/M*), which is the basic idea of [31]. The EM-type algorithms were also compared, which are denoted as *EM* for GMMs and *IRA* for other EMMs [13], [18].

#### A. Assessment over the proposed *Dadam* on the synthesis data

We first evaluated the effectiveness of our *Dadam* in adaptively accelerating the convergence. In this part, we only optimised the  $\Sigma_i$  whilst setting the  $\pi$  and  $\mu_i$  as the ground truth of the synthesis data. Fig. 1 illustrates the convergence speed. From this figure, we can clearly see that the optimisation on our established manifold exhibits much faster convergence. Furthermore, both the adaptive methods of [64] and the *Dadam* were shown to boost the speed. The proposed *Dadam* achieved the fastest convergence, which verifies the effectiveness of our directional adaptive method.

#### B. Overall comparisons on the synthesis data

We next compared our proposed algorithm (i.e., *W/M+Dadam*) with the *WO/M* and the *EM* methods under GMM problems. Similar results can be seen for other EMMs, and we list the result for GMMs in Table III. It

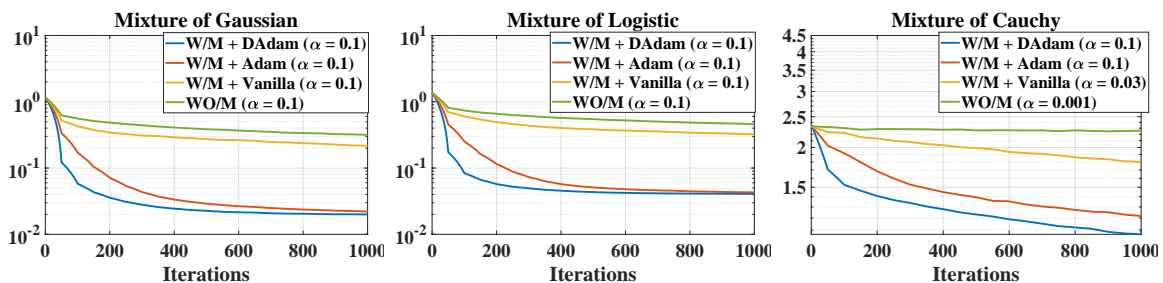


Fig. 1. The Wasserstein distance against the number of iterations for 4 algorithms, averaged by the 3 types of datasets ( $\{m, k\} = \{2, 3\}, \{8, 9\}, \{16, 27\}$ ). The best learning rate is shown in legends.

should be pointed out that all parameters ( $\pi$ ,  $\mu_i$  and  $\Sigma_i$ ) were optimised in this test and each result was reported based on the corresponding best learning rates. From this table, we can see that our algorithm not only achieves an extremely stable estimation (the lowest deviations) but also the lowest values in terms of both the Wasserstein distance and the NLL.

TABLE III  
COMPARISONS AMONG OUR, WO/M AND EM METHODS FOR GMMs BY VARYING  $m$  AND  $k$ .

	$m = 2, k = 3$		$m = 8, k = 9$		$m = 16, k = 27$	
	Wass	NLL	Wass	NLL	Wass	NLL
W/M+Dadam	<b>0.01 ± 0.00</b>	<b>5.10 ± 0.00</b>	<b>0.03 ± 0.03</b>	<b>19.49 ± 0.03</b>	<b>2.39 ± 0.33</b>	<b>44.92 ± 1.04</b>
WO/M	0.03 ± 0.00	5.12 ± 0.00	4.26 ± 3.61	22.27 ± 1.69	5e3 ± 589	Inf
EM	0.65 ± 1.06	5.30 ± 0.35	0.70 ± 0.46	19.83 ± 0.29	2.51 ± 1.27	48.84 ± 1.24

### C. Overall comparisons on the BSDS500

We then evaluated our algorithm on the BSDS500, and Table IV shows the results. From this table, we see some improvements of using the Wasserstein distance instead of the KL divergence, by comparing the *WO/M* with the IRA. However, due to the probability constraint, the *WO/M* is highly unstable and its fail ratio reaches  $> 50\%$  for the Gaussian mixture and Logistic mixture. More importantly, by optimising on our established manifold together with our *Dadam* method (denoted as *Our*), we can achieve the consistently best performances over the five metrics. Again, our algorithm also achieved highly stable estimation, taking advantages of the Wasserstein distance compared to the IRA working under the KL. Another advantage of our algorithm is its universal convergence, while the IRA does not converge for the mixture of *Gamma*, which limits the flexibility of EMMs.

TABLE IV  
COMPARISON VIA FIVE METRICS OF OUR, WO/M AND IRA ALGORITHMS OVER THE BSDS500 DATASET

	Gaussian Mixture			Logistic Mixture			Cauchy Mixture			Gamma Mixture		
	Our	WO/M	IRA	Our	WO/M	IRA	Our	WO/M	IRA	Our	WO/M	IRA
Wass	<b>35.0</b> $\pm 4.68$	89.5 $\pm 10.0$	53.6 $\pm 21.9$	<b>45.8</b> $\pm 12.7$	154 $\pm 10.9$	68.0 $\pm 24.2$	<b>179</b> $\pm 15.3$	211 $\pm 7.77$	253 $\pm 65.4$	<b>35.5</b> $\pm 1.82$	510 $\pm 71.2$	–
NLL	<b>11.8</b> $\pm 0.01$	12.2 $\pm 0.11$	11.8 $\pm 0.05$	<b>10.6</b> $\pm 0.02$	12.5 $\pm 0.25$	10.6 $\pm 0.06$	12.1 $\pm 0.01$	12.3 $\pm 0.01$	<b>12.0</b> $\pm 0.05$	<b>13.3</b> $\pm 0.07$	19.1 $\pm 0.86$	–
PSNR (dB)	<b>18.9</b> $\pm 0.07$	18.6 $\pm 0.18$	18.3 $\pm 0.66$	<b>18.8</b> $\pm 0.11$	18.2 $\pm 0.18$	17.8 $\pm 0.67$	19.3 $\pm 0.05$	<b>19.3</b> $\pm 0.06$	18.4 $\pm 0.56$	<b>21.0</b> $\pm 0.08$	18.0 $\pm 0.58$	–
SSIM	<b>0.68</b> $\pm 0.00$	0.65 $\pm 0.01$	0.66 $\pm 0.03$	<b>0.67</b> $\pm 0.01$	0.62 $\pm 0.01$	0.63 $\pm 0.03$	<b>0.70</b> $\pm 0.00$	0.70 $\pm 0.00$	0.69 $\pm 0.02$	<b>0.73</b> $\pm 0.00$	0.59 $\pm 0.03$	–
FailR	<b>0.20%</b>	53.1%	2.98%	<b>0.46%</b>	75.5%	2.68%	<b>1.16%</b>	0.82%	17.16%	<b>0%</b>	2.02%	100%

## VI. CONCLUSION

We have proposed a new and complete framework for solving general EMMs. To this end, we have first provided a unified summary of the existing flexible candidates for identifiable EMMs via the stochastic representation. Then, an approximate Wasserstein distance for EMMs has been proposed and the corresponding Riemannian metrics have been explicitly calculated. The so established manifold has been shown to consistently improve the optimisation for the above summarised EMMs, even when a vanilla Riemannian gradient descent is employed. We have further proposed a directional adaptively accelerated algorithm to enhance and stabilise the convergence, the performance of which has been validated through comprehensive experimental results.

## APPENDIX

### A. Proof for expressions in Table 1

As mentioned in the paper, we have  $p_{\mathcal{R}}(t) = g(t^2) \cdot t^{m-1}$ . The pdf of  $\mathcal{R}^2$  is then obtained accordingly as,

$$p_{\mathcal{R}^2}(t) = \frac{1}{2} \cdot g(t) \cdot t^{m/2-1}. \quad (8)$$

The term  $g(t)$  can be further decomposed as  $c \cdot g_c(t)$ , where  $g_c(t)$  is a nuclear term that only relates to  $t$ , and  $c$  is a normalisation term of  $p_{\mathcal{R}}(t)$ . This allows us to prove the results in Table 1 related to computable elliptical probability distribution functions (pdf) as follows.

- **Kotz type distributions:** The nuclear term of density generator is  $g_c(t) = t^{a-1}\exp(-bt^s)$  and  $c$  can be calculated from the condition as  $\int p_{\mathcal{R}}(t)dt = \int g(t^2) \cdot t^{m-1}dt = 1$  as,

$$c = \left( \int_0^\infty t^{2a+m-3}\exp(-bt^{2s})dt \right)^{-1} = \frac{2sb^{\frac{2a+m-2}{2s}}}{\Gamma(\frac{2a+m-2}{2s})}. \quad (9)$$

We now arrive at the pdf of  $\mathcal{R}^2$  for the Kotz type distributions, in the form

$$p_{\mathcal{R}^2}(t) = \frac{sb^{\frac{2a+m-2}{2s}}}{\Gamma(\frac{2a+m-2}{2s})} t^{\frac{m}{2}+a-2}\exp(-bt^s). \quad (10)$$

However, in practice, it is intractable to generate samples of  $\mathcal{R}^2$  as in (10). On the other hand, it can be found that  $\mathcal{G}^{1/s}$  has the same distribution as  $\mathcal{R}^2$  when  $\mathcal{G}$  is Gamma distributed. Specifically, when  $\mathcal{G} \sim \text{Ga}(\frac{2a+m-2}{2s}, b)$ , we obtain the pdf of  $\mathcal{G}^{1/s}$  as,

$$p_{\mathcal{G}^{1/s}}(t) = st^{s-1} \frac{b^{\frac{2a+m-2}{2s}} t^{\frac{2a+m-2}{2}-s}\exp(-bt^s)}{\Gamma(\frac{2a+m-2}{2s})} = \frac{sb^{\frac{2a+m-2}{2s}}}{\Gamma(\frac{2a+m-2}{2s})} t^{\frac{m}{2}+a-2}\exp(-bt^s). \quad (11)$$

This proves that  $\mathcal{R}^2 \stackrel{d}{=} \mathcal{G}^{1/s}$  for the Kotz type distributions.

- **Scale mixture of normals distributions:** The scale mixture of normal distributions consists of a mixture of zero-mean normal distributions (denoted as  $\mathcal{X} = \sqrt{\mathcal{K}}\mathcal{N}$ , where  $\mathcal{N}$  is zero-mean normal distribution and  $\mathcal{K}$  is called the mixing distribution with pdf  $p_{\mathcal{K}}(t)$ ). Correspondingly, we can write the pdf of  $\mathcal{X}$  as

$$p_{\mathcal{X}}(\mathbf{x}) = \int_t p_{\mathcal{X}}(\mathbf{x}|t)p_{\mathcal{K}}(t)dt \propto \int_t t^{-\frac{m}{2}} \exp\left(\frac{\mathbf{x}^T \boldsymbol{\Sigma}^{-1} \mathbf{x}}{t}\right) p_{\mathcal{K}}(t)dt. \quad (12)$$

Furthermore, to represent a scale mixture of normal distributions in the form of stochastic representations, by inspection we see that the normal distribution  $\mathcal{N}$  can be represented by a multiplication of  $\sqrt{\chi_m^2}$  and  $\mathcal{S}$  (from the stochastic representation), so that the following holds:

$$\mathcal{X} = \sqrt{\mathcal{K}}\mathcal{N} = \sqrt{\mathcal{K} \cdot \chi_m^2} \cdot \mathcal{S} = \sqrt{\mathcal{K} \cdot \mathcal{G}}\mathcal{S}, \quad (13)$$

where  $\mathcal{G} \sim \text{Ga}(m/2, 2)$ . In this case,  $\mathcal{R}^2 \stackrel{d}{=} \mathcal{K} \cdot \mathcal{G}$  by the stochastic representation. Therefore, although (12) and (13) are equivalent, (13) provides a unified stochastic representation within the elliptical family. This allows us to discuss different  $\mathcal{K}$  for different sub-classes of scale mixture normals in the following.

For the Pearson type VII distributions where the nuclear density generator is given by  $g_c(t) = (1 + t/v)^{-s}$ , we can obtain the corresponding normalisation term  $c$  as follows,

$$c = \left( \int_0^\infty t^{m-1}(1 + t^2/v)^{-s} dt \right)^{-1} = \frac{2\Gamma(s)}{(v)^{m/2}\Gamma(s - m/2)\Gamma(m/2)}. \quad (14)$$

Consequently, the pdf of  $\mathcal{R}^2$  becomes:

$$p_{\mathcal{R}^2}(t) = \frac{\Gamma(s)}{\Gamma(s - \frac{m}{2})\Gamma(\frac{m}{2})v^{\frac{m}{2}}} \left(1 + \frac{t}{v}\right)^{-s} t^{\frac{m}{2}-1}. \quad (15)$$

Again, the rather complicated form of (15) makes it impossible to generate samples. It can be found that when  $p_{\mathcal{K}}(t) = \frac{(2v)^{s-m/2}}{\Gamma(s-m/2)} t^{m/2-s-1} \exp(-2v/t)$  and  $\mathcal{G} \sim \text{Ga}(m/2, 2)$ ,  $\mathcal{R}^2$  in (15) has the same pdf as  $\mathcal{K} \cdot \mathcal{G}$ . This can be verified as follows,

$$\begin{aligned} p_{\mathcal{R}^2}(t) &= \int_0^\infty p_{\mathcal{G}}(t|\tau) p_{\mathcal{K}}(\tau) d\tau = \int_0^\infty \frac{\left(\frac{2}{\tau}\right)^{\frac{m}{2}} t^{\frac{m}{2}-1} \exp(-\frac{2t}{\tau})}{\Gamma(\frac{m}{2})} \cdot \frac{(2v)^{s-\frac{m}{2}}}{\Gamma(s-\frac{m}{2})} \tau^{\frac{m}{2}-s-1} \exp(-\frac{2v}{\tau}) d\tau \\ &= \frac{\Gamma(s) t^{\frac{m}{2}-1}}{\Gamma(s-\frac{m}{2}) \Gamma(\frac{m}{2}) v^{\frac{m}{2}} (1+\frac{t}{v})^s}, \end{aligned} \quad (16)$$

where  $\mathcal{K}^{-1} \sim \text{Ga}(s - \frac{m}{2}, 2v)$  and  $\mathcal{R}^2 = {}^d \mathcal{K} \cdot \mathcal{G}$ .

Moreover, for other types within the scale mixture normals, Barndorff *et al.* [42] have proved that the generalised hyperbolic distributions can be formulated in the form of (12) when  $\mathcal{K}$  satisfies the inverse-Gaussian distribution. The elliptical logistic distributions are also mixtures of normals, where  $\sqrt{\mathcal{K}}$  in (12) relates to the Kolmogorov-Smirnov distribution [44]. Besides, the relationship between the scale mixture normals and the  $\alpha$ -stable distribution is given in [21], which satisfies our equivalent form of (13). We omit the tedious proofs here.

- **Pearson type II distributions:** The nuclear density generator is  $g_c(t) = (1-t)^{s-1}$  with the constraint  $t \in [0, 1]$ . We omit the proof here because the calculation of  $c$  and the pdf of  $\mathcal{R}^2$  are well documented in [38].

This completes the proof of Table 1.

### B. Proof of Theorem 1

**Symmetry:** It is easy to verify the symmetry of  $d_U(\mathcal{Y}_1, \mathcal{Y}_2)$ , i.e.,  $d_U(\mathcal{Y}_1, \mathcal{Y}_2) = d_U(\mathcal{Y}_2, \mathcal{Y}_1)$ .

**Non-negativity:** Due to  $\arccos(\cdot) \geq 0$ ,  $d_W^2(\mathcal{X}_{i,1}, \mathcal{X}_{j,2}) \geq 0$  and  $\gamma(i, j) \geq 0$  for all  $i, j$ ,  $d_U(\mathcal{Y}_1, \mathcal{Y}_2) \geq 0$ . More importantly, the equality holds if and only if  $\mathcal{Y}_1 = {}^d \mathcal{Y}_2$ . In this case,  $\min_{\gamma(i,j)} \sum_{i,j} \frac{\gamma(i,j)}{k} d_W^2(\mathcal{X}_{i,1}, \mathcal{X}_{j,2}) = 0$  and  $\min_{\gamma(i,j)} \arccos(\sum_{i,j} \gamma(i,j) \sqrt{\pi_{i,1} \pi_{j,2}}) = \arccos(\sum_i \pi_{i,1}) = \arccos(1) = 0$ , which results in  $d_U(\mathcal{Y}_1, \mathcal{Y}_2) = 0$ .

**Triangle inequality:** Because  $\gamma(i, j)$  is binary  $\in \{0, 1\}$  for each pair  $\{i, j\}$ , and it satisfies  $\sum_{i=1}^k \gamma(i, j) = 1$  and  $\sum_{j=1}^k \gamma(i, j) = 1$ , the  $\gamma(i, j)$  operates as a bijection between the elliptical distributions within the first and second EMMs.

Then, in order to prove the triangle property, we denote the third EMM as  $\mathcal{Y}_3 = {}^d \sum_{h=1}^k z_{h,3} \mathcal{X}_{h,3}$ , and investigate the relationship between  $d_U(\mathcal{Y}_1, \mathcal{Y}_2)$  and  $d_U(\mathcal{Y}_1, \mathcal{Y}_3) + d_U(\mathcal{Y}_2, \mathcal{Y}_3)$ . We use  $\gamma^*(\cdot, \cdot)$  to denote the optimal  $\gamma(\cdot, \cdot)$  in the defined distance  $d_U(\cdot, \cdot)$ , and also define the following function

$$f(\mathcal{Y}_1, \mathcal{Y}_2, \gamma(i, j)) = \sum_{i,j} \gamma(i, j) d_W^2(\mathcal{X}_{i,1}, \mathcal{X}_{j,2}) + \arccos\left(\sum_{i,j} \gamma(i, j) \sqrt{\pi_{i,1} \pi_{j,2}}\right). \quad (17)$$

By Definition 1,  $\min_{\gamma(i,j)} f(\mathcal{Y}_1, \mathcal{Y}_2, \gamma(i, j)) = f(\mathcal{Y}_1, \mathcal{Y}_2, \gamma^*(i, j)) = d_U(\mathcal{Y}_1, \mathcal{Y}_2)$ .

More importantly, for two arbitrary  $\gamma(i, h)$  and  $\gamma(h, j)$ , their combination  $\gamma(i, h) \cap \gamma(h, j) = \sum_{h=1}^k \gamma(i, h) \cdot \gamma(h, j)$  also formulates a transport plan  $\gamma(i, j)$  because  $\gamma(i, h) \cap \gamma(h, j)$  is still binary and  $\sum_{i=1}^k \gamma(i, h) \cap \gamma(h, j) = \sum_{j=1}^k \gamma(i, h) \cap \gamma(h, j) = 1$ .

We therefore now arrive at

$$\begin{aligned}
d_U(\mathcal{Y}_1, \mathcal{Y}_3) + d_U(\mathcal{Y}_2, \mathcal{Y}_3) &= f(\mathcal{Y}_1, \mathcal{Y}_3, \gamma^*(i, h)) + f(\mathcal{Y}_2, \mathcal{Y}_3, \gamma^*(j, h)) \\
&= \frac{1}{k} \left( \sum_{i,h} \gamma^*(i, h) d_W^2(\mathcal{X}_{i,1}, \mathcal{X}_{h,3}) + \sum_{h,j} \gamma^*(h, j) d_W^2(\mathcal{X}_{h,3}, \mathcal{X}_{j,2}) \right) \\
&\quad + \arccos\left(\sum_{i,h} \gamma^*(i, h) \sqrt{\pi_{i,1} \pi_{h,3}}\right) + \arccos\left(\sum_{h,j} \gamma^*(h, j) \sqrt{\pi_{h,3} \pi_{j,2}}\right) \\
&\geq \frac{1}{k} \sum_{i,j} (\gamma^*(i, h) \cap \gamma^*(h, j)) d_W^2(\mathcal{X}_{i,1}, \mathcal{X}_{j,2}) + \arccos\left(\sum_{i,j} (\gamma^*(i, h) \cap \gamma^*(h, j)) \sqrt{\pi_{i,1} \pi_{j,2}}\right) \quad (18) \\
&= f(\mathcal{Y}_1, \mathcal{Y}_2, \gamma^*(i, h) \cap \gamma^*(h, j)) \\
&\geq f(\mathcal{Y}_1, \mathcal{Y}_2, \gamma^*(i, j)) \\
&= d_U(\mathcal{Y}_1, \mathcal{Y}_2).
\end{aligned}$$

In (18), the first inequality holds due to the fact that both  $d_W^2(\mathcal{X}_{i,1}, \mathcal{X}_{j,2})$  and  $\arccos(\sum_{i,j} \gamma(i, j) \sqrt{\pi_{i,1} \pi_{j,2}})$  satisfy the triangle property. Moreover, the second inequality is due to the fact that the combined plan  $\gamma(i, h) \cap \gamma(h, j)$  is not necessarily the optimal plan between  $\mathcal{Y}_1$  and  $\mathcal{Y}_2$ , as the optimal plan  $\gamma^*(i, j)$  achieves the minimum and defines the distance of  $d_U(\mathcal{Y}_1, \mathcal{Y}_2)$ .

This completes the proof of Theorem 1.

### C. Proof of Lemma 1

Recall that  $\mathcal{Y} \sim \sum_{i=1}^k \pi_i \mathcal{E}(\mathbf{x} | \boldsymbol{\mu}_i, \boldsymbol{\Sigma}_i, \mathcal{R})$ . We can now write the definition of the Wasserstein distance in the form

$$d_W^2(\mathcal{Y}_1, \mathcal{Y}_2) = \inf_{\eta(\mathcal{Y}_1, \mathcal{Y}_2)} \int_{m \times m} \eta(\mathcal{Y}_1, \mathcal{Y}_2) \|\mathbf{x}_1 - \mathbf{x}_2\|_2^2 d\mathbf{x}_1 d\mathbf{x}_2, \quad (19)$$

where  $\eta(\mathcal{Y}_1, \mathcal{Y}_2)$  denotes the joint distribution between  $\mathcal{Y}_1$  and  $\mathcal{Y}_2$ , and satisfies  $\int_m \eta(\mathcal{Y}_1, \mathcal{Y}_2) d\mathbf{x}_1 = p_{\mathcal{Y}_2}(\mathbf{x}_2)$  and  $\int_m \eta(\mathcal{Y}_1, \mathcal{Y}_2) d\mathbf{x}_2 = p_{\mathcal{Y}_1}(\mathbf{x}_1)$ .

More importantly,

$$\begin{aligned}
\sum_{i,j} \frac{\gamma^*(i, j)}{k} d_W^2(\mathcal{X}_{i,1}, \mathcal{X}_{j,2}) &= \sum_{i,j} \frac{\gamma^*(i, j)}{k} \inf_{\eta(\mathcal{X}_{i,1}, \mathcal{X}_{j,2})} \int_{m \times m} \eta(\mathcal{X}_{i,1}, \mathcal{X}_{j,2}) \|\mathbf{x}_1 - \mathbf{x}_2\|_2^2 d\mathbf{x}_1 d\mathbf{x}_2 \\
&= \int_{m \times m} \sum_{i,j} \frac{\gamma^*(i, j)}{k} \eta^*(\mathcal{X}_{i,1}, \mathcal{X}_{j,2}) \|\mathbf{x}_1 - \mathbf{x}_2\|_2^2 d\mathbf{x}_1 d\mathbf{x}_2, \quad (20)
\end{aligned}$$

where  $\eta^*(\mathcal{X}_{i,1}, \mathcal{X}_{j,2})$  is the optimal plan that achieves the Wasserstein distance between  $\mathcal{X}_{i,1}$  and  $\mathcal{X}_{j,2}$ . Therefore, by comparing (19) and (20), we can easily observe that  $\sum_{i,j} \frac{\gamma^*(i, j)}{k} \eta^*(\mathcal{X}_{i,1}, \mathcal{X}_{j,2})$  consists a subset of joint distribution of  $\eta(\mathcal{Y}_1, \mathcal{Y}_2)$ , due to  $\pi_{i,1} = \pi_{j,2} = 1/k$ . In other words, because of the factorisation from  $\mathcal{Y}$  to  $\mathcal{X}$ , the  $\sum_{i,j} \frac{\gamma^*(i, j)}{k} \eta^*(\mathcal{X}_{i,1}, \mathcal{X}_{j,2})$  does not necessarily achieve the optimal transport plan between  $\mathcal{Y}_1$  and  $\mathcal{Y}_2$ .

Moreover, for balanced EMMs, the following holds for arbitrary  $\gamma(i, j)$ ,

$$\arccos\left(\sum_{i,j} \gamma(i, j) \sqrt{\pi_{i,1} \pi_{j,2}}\right) = 0. \quad (21)$$



Thus, we have

$$d_W^2(\mathcal{Y}_1, \mathcal{Y}_2) \leq \sum_{i,j} \frac{\gamma^*(i,j)}{k} d_W^2(\mathcal{X}_{i,1}, \mathcal{X}_{j,2}) = d_U(\mathcal{Y}_1, \mathcal{Y}_2). \quad (22)$$

This completes the proof of Lemma 1.

#### D. Proof of Lemma 2

Due to the fact that  $\gamma(i, j)$  in Definition 1 is a bijection between mixture components in  $\mathcal{Y}_1$  and  $\mathcal{Y}_2$ , for each  $\pi_1, \mu_{i,1}$  and  $\Sigma_{i,1}$  in  $\mathcal{Y}_1$ , there exist only one corresponding  $\pi_2, \mu_{j,2}$  and  $\Sigma_{j,2}$ , respectively, in  $\mathcal{Y}_2$ . In other words, when casting the problem to the parametric space, the Hessian of  $d_U(\mathcal{Y}_\theta, \mathcal{Y}_{\theta+s\Delta\theta})$  can be calculated as follows,

$$\frac{\partial^2 d_U(\mathcal{Y}_\theta, \mathcal{Y}_{\theta+s\Delta\theta})}{\partial s^2} \Big|_{s \rightarrow 0} = \frac{1}{k} \sum_{i=1}^K \frac{\partial^2 d_W^2(\mathcal{X}_{\mu_i, \Sigma_i}, \mathcal{X}_{\mu_i+s\Delta\mu_i, \Sigma_i+s\Delta\Sigma_i})}{\partial s^2} \Big|_{s \rightarrow 0} + \frac{\partial^2 \arccos(\sqrt{\pi}^T (\sqrt{\pi + s\Delta\pi}))}{\partial s^2} \Big|_{s \rightarrow 0}, \quad (23)$$

where the square root operation  $\sqrt{\cdot}$  is performed element-wise.

In (23), we can see that the manifold defined by  $d_U(\mathcal{Y}_\theta, \mathcal{Y}_{\theta+\Delta\theta})$  is a product manifold defined by  $d_W^2(\mathcal{X}_{\mu_i, \Sigma_i}, \mathcal{X}_{\mu_i+\Delta\mu_i, \Sigma_i+\Delta\Sigma_i})$  and  $\arccos(\sqrt{\pi}^T (\sqrt{\pi + \Delta\pi}))$ .

Furthermore,  $\arccos(\sqrt{\pi}^T (\sqrt{\pi + \Delta\pi}))$  defines a sphere manifold [57] (Examples 3.5.1 and 3.6.1), for which basic operations are provided in Examples 4.1.1, 5.4.1 and 8.1.7 of [57]. On the other hand, the Wasserstein distance between two elliptical distributions has an explicit representation as follows [50], [51],

$$d_W^2(\mathcal{X}_{\mu_i, \Sigma_i}, \mathcal{X}_{\mu_i+\Delta\mu_i, \Sigma_i+\Delta\Sigma_i}) = \|\Delta\mu_i\|_2^2 + \frac{\mathbb{E}[\mathcal{R}^2]}{m} \text{tr}(\Sigma_i + (\Sigma_i + \Delta\Sigma_i) - 2(\Sigma_i^{1/2} (\Sigma_i + \Delta\Sigma_i) \Sigma_i^{1/2})^{1/2}). \quad (24)$$

We can thus conclude that the manifold for  $\mu_i$  is the conventional Euclidean space within  $\mathbb{R}^m$ . Moreover, the manifold of  $\Sigma_i$  can also be correspondingly obtained on the basis of [53].

This completes the proof of Lemma 2.

#### E. Calculations within Table 2

The basic operations on a sphere manifold were described in [57] (Examples 3.5.1, 3.6.1, 4.1.1, 5.4.1 and 8.1.7). As the manifold for  $\mu_i$  is the conventional Euclidean space, the trivial gradient descent can be employed. Operations for  $\Sigma_i$  under the Wasserstein manifold can be found in [53]. Furthermore, we omit the scale weight  $\frac{\mathbb{E}[\mathcal{R}^2]}{m}$  in our work as it can be incorporated into the stepsize  $\alpha$  during the gradient descent.

To calculate the Euclidean gradients, we first explicitly express our cost function, i.e., the sliced Wasserstein distance  $d_{SW}(\mathcal{Y}_\theta, \mathcal{Y}^*)$ , as follows,

$$d_{SW}(\mathcal{Y}_\theta, \mathcal{Y}^*) = \int_m \inf_{\eta(\text{Ra}(\mathcal{Y}_\theta, \mathbf{p}), \text{Ra}(\mathcal{Y}^*, \mathbf{p}))} \int_{\mathbb{R} \times \mathbb{R}} \eta(\text{Ra}(\mathcal{Y}_\theta, \mathbf{p}), \text{Ra}(\mathcal{Y}^*, \mathbf{p}))(y_1 - y_2)^2 dy_1 dy_2 d\mathbf{p}, \quad (25)$$

where  $y_1$  denotes the Radon transform [56]  $\text{Ra}(\mathcal{Y}_\theta, \mathbf{p})$ , which projects  $\mathcal{Y}_\theta$  onto a one-dimensional random variable along the direction  $\mathbf{p}$ . Similarly,  $y_2$  denotes the Radon transform of  $\mathcal{Y}^*$  with the direction  $\mathbf{p}$ . Recall that  $\eta(\cdot, \cdot)$  is a joint distribution. Due to the fact that elliptical distributions belong to the location-scale family, as

described by the stochastic representation, the Radon transform of each  $\mathcal{X}_{\boldsymbol{\mu}_i, \boldsymbol{\Sigma}_i}$  has a simple representation in the form  $\mathcal{X}_{\mathbf{p}^T \boldsymbol{\mu}_i, \mathbf{p}^T \boldsymbol{\Sigma}_i \mathbf{p}} \sim \mathcal{E}(x; \mathbf{p}^T \boldsymbol{\mu}_i, \mathbf{p}^T \boldsymbol{\Sigma}_i \mathbf{p}, \mathcal{R})$ , where  $\mathcal{X}$  is a one-dimensional elliptical distribution.

Fortunately, the one-dimensional Wasserstein distance has the closed-form solution [30], we can re-write (25) as

$$\min_{\boldsymbol{\pi}, \boldsymbol{\mu}_i, \boldsymbol{\Sigma}_i} d_{SW}(\mathcal{Y}_{\boldsymbol{\theta}}, \mathcal{Y}^*) = \min_{\boldsymbol{\pi}, \boldsymbol{\mu}_i, \boldsymbol{\Sigma}_i} \int_m \int_{\mathbb{R}} |y - T(y)|^2 \sum_{i=1}^k c_m \pi_i \cdot (\mathbf{p}^T \boldsymbol{\Sigma}_i^h \mathbf{p})^{-\frac{1}{2}} g\left(\frac{(y - \mathbf{p}^T \boldsymbol{\mu}_i)^2}{\mathbf{p}^T \boldsymbol{\Sigma}_i^h \mathbf{p}}\right) dy d\mathbf{p}, \quad (26)$$

where  $T(y)$  is the optimal transport plan between  $\text{Ra}(\mathcal{Y}_{\boldsymbol{\theta}}, \mathbf{p})$  and  $\text{Ra}(\mathcal{Y}^*, \mathbf{p})$ , which can be explicitly obtained via their cumulative distribution functions [37]. When optimising (26) using stochastic gradient descent, for each  $\mathbf{p}$ , we therefore minimise

$$\min_{\boldsymbol{\pi}, \boldsymbol{\mu}_i, \boldsymbol{\Sigma}_i} J(\boldsymbol{\theta}, \mathbf{p}) = \min_{\boldsymbol{\pi}, \boldsymbol{\mu}_i, \boldsymbol{\Sigma}_i} \int_{\mathbb{R}} |y - T(y)|^2 \sum_{i=1}^k c_m \pi_i \cdot (\mathbf{p}^T \boldsymbol{\Sigma}_i^h \mathbf{p})^{-\frac{1}{2}} g\left(\frac{(y - \mathbf{p}^T \boldsymbol{\mu}_i)^2}{\mathbf{p}^T \boldsymbol{\Sigma}_i^h \mathbf{p}}\right) dy. \quad (27)$$

Then, by calculating the derivatives with regard to  $\sqrt{\pi_i}$ ,  $\boldsymbol{\mu}_i$  and  $\boldsymbol{\Sigma}_i$ , and upon introducing the Kantorovich potential  $\phi(y)$  [37], we obtain the Euclidean gradients as follows,

$$\nabla_{\sqrt{\pi_i}, \boldsymbol{\mu}_i, \boldsymbol{\Sigma}_i} J(\boldsymbol{\theta}, \mathbf{p}) = \int_{\mathbb{R}} \phi(y) \cdot \nabla_{\sqrt{\pi_i}, \boldsymbol{\mu}_i, \boldsymbol{\Sigma}_i} \left( \sum_{i=1}^k c_m \sqrt{\pi_i}^2 \cdot (\mathbf{p}^T \boldsymbol{\Sigma}_i^h \mathbf{p})^{-\frac{1}{2}} g\left(\frac{(y - \mathbf{p}^T \boldsymbol{\mu}_i)^2}{\mathbf{p}^T \boldsymbol{\Sigma}_i^h \mathbf{p}}\right) \right) dy, \quad (28)$$

where  $\nabla_{\sqrt{\pi_i}, \boldsymbol{\mu}_i, \boldsymbol{\Sigma}_i}(\cdot)$  denotes the derivatives with regard to  $\{\sqrt{\pi_i}, \boldsymbol{\mu}_i, \boldsymbol{\Sigma}_i\}$ , respectively. The Euclidean gradients in the Table 2 can then be easily calculated.

## REFERENCES

- [1] X. J. Zhu, “Semi-supervised learning literature survey,” University of Wisconsin-Madison Department of Computer Sciences, Tech. Rep., 2005.
- [2] G. E. Hinton, S. Sabour, and N. Frosst, “Matrix capsules with EM routing,” 2018.
- [3] F. Chen, L. Zhang, and H. Yu, “External patch prior guided internal clustering for image denoising,” in *Proceedings of the IEEE International Conference on Computer Vision*, 2015, pp. 603–611.
- [4] J. Goldberger, S. Gordon, and H. Greenspan, “An efficient image similarity measure based on approximations of KL-divergence between two Gaussian mixtures,” in *null*. IEEE, 2003, p. 487.
- [5] B. Jian and B. C. Vemuri, “Robust point set registration using gaussian mixture models,” *IEEE Transactions on Pattern Analysis and Machine Intelligence*, vol. 33, no. 8, pp. 1633–1645, 2011.
- [6] L. Xu and M. I. Jordan, “On convergence properties of the EM algorithm for gaussian mixtures,” *Neural Computation*, vol. 8, no. 1, pp. 129–151, 1996.
- [7] R. A. Redner and H. F. Walker, “Mixture densities, maximum likelihood and the em algorithm,” *SIAM Review*, vol. 26, no. 2, pp. 195–239, 1984.
- [8] R. Hosseini and S. Sra, “Matrix manifold optimization for Gaussian mixtures,” in *Advances in Neural Information Processing Systems*, 2015, pp. 910–918.
- [9] —, “An alternative to EM for Gaussian mixture models: Batch and stochastic riemannian optimization,” *arXiv preprint arXiv:1706.03267*, 2017.
- [10] M. I. Jordan and R. A. Jacobs, “Hierarchical mixtures of experts and the EM algorithm,” *Neural computation*, vol. 6, no. 2, pp. 181–214, 1994.

- [11] I. Naim and D. Gildea, “Convergence of the EM algorithm for gaussian mixtures with unbalanced mixing coefficients,” *arXiv preprint arXiv:1206.6427*, 2012.
- [12] R. Salakhutdinov, S. T. Roweis, and Z. Ghahramani, “Optimization with EM and expectation-conjugate-gradient,” in *Proceedings of the 20th International Conference on Machine Learning (ICML-03)*, 2003, pp. 672–679.
- [13] D. Peel and G. J. McLachlan, “Robust mixture modelling using the t distribution,” *Statistics and Computing*, vol. 10, no. 4, pp. 339–348, 2000.
- [14] J. L. Andrews and P. D. McNicholas, “Model-based clustering, classification, and discriminant analysis via mixtures of multivariate t-distributions,” *Statistics and Computing*, vol. 22, no. 5, pp. 1021–1029, 2012.
- [15] T.-I. Lin, P. D. McNicholas, and H. J. Ho, “Capturing patterns via parsimonious t mixture models,” *Statistics & Probability Letters*, vol. 88, pp. 80–87, 2014.
- [16] S. Tan and L. Jiao, “Multivariate statistical models for image denoising in the wavelet domain,” *International Journal of Computer Vision*, vol. 75, no. 2, pp. 209–230, 2007.
- [17] R. P. Browne and P. D. McNicholas, “A mixture of generalized hyperbolic distributions,” *Canadian Journal of Statistics*, vol. 43, no. 2, pp. 176–198, 2015.
- [18] J. T. Kent and D. E. Tyler, “Redescending M-estimates of multivariate location and scatter,” *The Annals of Statistics*, pp. 2102–2119, 1991.
- [19] T. Zhang, A. Wiesel, and M. S. Greco, “Multivariate generalized Gaussian distribution: Convexity and graphical models,” *IEEE Transactions on Signal Processing*, vol. 61, no. 16, pp. 4141–4148, 2013.
- [20] S. Sra and R. Hosseini, “Geometric optimisation on positive definite matrices for elliptically contoured distributions,” in *Advances in Neural Information Processing Systems*, 2013, pp. 2562–2570.
- [21] D. F. Andrews and C. L. Mallows, “Scale mixtures of normal distributions,” *Journal of the Royal Statistical Society. Series B (Methodological)*, pp. 99–102, 1974.
- [22] J. Xu, D. J. Hsu, and A. Maleki, “Global analysis of expectation maximization for mixtures of two gaussians,” in *Advances in Neural Information Processing Systems*, 2016, pp. 2676–2684.
- [23] C. Jin, Y. Zhang, S. Balakrishnan, M. J. Wainwright, and M. I. Jordan, “Local maxima in the likelihood of Gaussian mixture models: Structural results and algorithmic consequences,” in *Advances in Neural Information Processing Systems*, 2016, pp. 4116–4124.
- [24] G. Monge, *Mémoire sur la théorie des déblais et des remblais*. De l’Imprimerie Royale, 1781.
- [25] L. Kantorovich, “On the transfer of masses: Doklady akademii nauk ussr,” 1942.
- [26] C. Villani, *Optimal transport: old and new*. Springer Science & Business Media, 2008, vol. 338.
- [27] I. Gulrajani, F. Ahmed, M. Arjovsky, V. Dumoulin, and A. C. Courville, “Improved training of wasserstein gans,” in *Advances in Neural Information Processing Systems*, 2017, pp. 5767–5777.
- [28] M. Arjovsky, S. Chintala, and L. Bottou, “Wasserstein gan,” *arXiv preprint arXiv:1701.07875*, 2017.
- [29] G. Montavon, K.-R. Müller, and M. Cuturi, “Wasserstein training of restricted boltzmann machines,” in *Advances in Neural Information Processing Systems*, 2016, pp. 3718–3726.
- [30] S. Kolouri, S. R. Park, M. Thorpe, D. Slepcev, and G. K. Rohde, “Optimal mass transport: Signal processing and machine-learning applications,” *IEEE Signal Processing Magazine*, vol. 34, no. 4, pp. 43–59, 2017.
- [31] S. Kolouri, G. K. Rohde, and H. Hoffmann, “Sliced wasserstein distance for learning gaussian mixture models,” in *Proceedings of the IEEE Conference on Computer Vision and Pattern Recognition*, 2018, pp. 3427–3436.
- [32] S.-I. Amari, “Natural gradient works efficiently in learning,” *Neural Computation*, vol. 10, no. 2, pp. 251–276, 1998.
- [33] J. Martens, “New insights and perspectives on the natural gradient method,” *arXiv preprint arXiv:1412.1193*, 2014.
- [34] W. Wang, R. Wang, Z. Huang, S. Shan, and X. Chen, “Discriminant analysis on Riemannian manifold of Gaussian distributions for face recognition with image sets,” in *Proceedings of the IEEE Conference on Computer Vision and Pattern Recognition*, 2015, pp. 2048–2057.

- [35] A. M. Peter and A. Rangarajan, “Information geometry for landmark shape analysis: Unifying shape representation and deformation,” *IEEE Transactions on Pattern Analysis and Machine Intelligence*, vol. 31, no. 2, pp. 337–350, 2009.
- [36] F. Nielsen and R. Nock, “On  $w$ -mixtures: Finite convex combinations of prescribed component distributions,” *arXiv preprint arXiv:1708.00568*, 2017.
- [37] Y. Chen and W. Li, “Natural gradient in Wasserstein statistical manifold,” *arXiv preprint arXiv:1805.08380*, 2018.
- [38] K. W. Fang, S. Kotz, and K. W. Ng, *Symmetric multivariate and related distributions*. London, U.K.: Chapman & Hall, 1990.
- [39] S. Cambanis, S. Huang, and G. Simons, “On the theory of elliptically contoured distributions,” *Journal of Multivariate Analysis*, vol. 11, no. 3, pp. 368–385, 1981.
- [40] G. Frahm, “Generalized elliptical distributions: Theory and applications,” Ph.D. dissertation, Universität zu Köln, 2004.
- [41] H. Holzmann, A. Munk, and T. Gneiting, “Identifiability of finite mixtures of elliptical distributions,” *Scandinavian journal of statistics*, vol. 33, no. 4, pp. 753–763, 2006.
- [42] O. Barndorff-Nielsen, J. Kent, and M. Sørensen, “Normal variance-mean mixtures and  $z$  distributions,” *International Statistical Review/Revue Internationale de Statistique*, pp. 145–159, 1982.
- [43] E. Ollila, D. E. Tyler, V. Koivunen, and H. V. Poor, “Complex elliptically symmetric distributions: Survey, new results and applications,” *IEEE Transactions on Signal Processing*, vol. 60, no. 11, pp. 5597–5625, 2012.
- [44] L. A. Stefanski, “A normal scale mixture representation of the logistic distribution,” *Statistics & Probability Letters*, vol. 11, no. 1, pp. 69–70, 1991.
- [45] F. Otto, “The geometry of dissipative evolution equations: the porous medium equation,” 2001.
- [46] S. Gallot, D. Hulin, and J. Lafontaine, “Curvature,” in *Riemannian Geometry*. Springer, 2004, pp. 129–206.
- [47] C. R. Givens, R. M. Shortt *et al.*, “A class of Wasserstein metrics for probability distributions.” *The Michigan Mathematical Journal*, vol. 31, no. 2, pp. 231–240, 1984.
- [48] M. Knott and C. S. Smith, “On the optimal mapping of distributions,” *Journal of Optimization Theory and Applications*, vol. 43, no. 1, pp. 39–49, 1984.
- [49] D. Dowson and B. Landau, “The fréchet distance between multivariate normal distributions,” *Journal of Multivariate Analysis*, vol. 12, no. 3, pp. 450–455, 1982.
- [50] N. Ghaffari and S. Walker, “On multivariate optimal transportation,” *arXiv preprint arXiv:1801.03516*, 2018.
- [51] B. Muzellec and M. Cuturi, “Generalizing point embeddings using the wasserstein space of elliptical distributions,” in *Advances in Neural Information Processing Systems*, 2018, pp. 10 237–10 248.
- [52] A. Takatsu *et al.*, “Wasserstein geometry of Gaussian measures,” *Osaka Journal of Mathematics*, vol. 48, no. 4, pp. 1005–1026, 2011.
- [53] L. Malagò, L. Montrucchio, and G. Pistone, “Wasserstein Riemannian geometry of Gaussian densities,” *Information Geometry*, vol. 1, no. 2, pp. 137–179, 2018.
- [54] S. Sra and R. Hosseini, “Conic geometric optimization on the manifold of positive definite matrices,” *SIAM Journal on Optimization*, vol. 25, no. 1, pp. 713–739, 2015.
- [55] K.-T. Sturm *et al.*, “On the geometry of metric measure spaces,” *Acta Mathematica*, vol. 196, no. 1, pp. 65–131, 2006.
- [56] J. Rabin, G. Peyré, J. Delon, and M. Bernot, “Wasserstein barycenter and its application to texture mixing,” in *International Conference on Scale Space and Variational Methods in Computer Vision*. Springer, 2011, pp. 435–446.
- [57] P.-A. Absil, R. Mahony, and R. Sepulchre, *Optimization algorithms on matrix manifolds*. Princeton University Press, 2009.
- [58] B. Lévy, “A numerical algorithm for L2 semi-discrete optimal transport in 3d,” *ESAIM: Mathematical Modelling and Numerical Analysis*, vol. 49, no. 6, pp. 1693–1715, 2015.
- [59] Y. Liu, F. Shang, J. Cheng, H. Cheng, and L. Jiao, “Accelerated first-order methods for geodesically convex optimization on riemannian manifolds,” in *Advances in Neural Information Processing Systems*, 2017, pp. 4868–4877.
- [60] H. Zhang, S. J. Reddi, and S. Sra, “Riemannian SVRG: Fast stochastic optimization on Riemannian manifolds,” in *Advances in Neural Information Processing Systems*, 2016, pp. 4592–4600.

- [61] H. Zhang and S. Sra, “First-order methods for geodesically convex optimization,” in *Conference on Learning Theory*, 2016, pp. 1617–1638.
- [62] S. J. Reddi, A. Hefny, S. Sra, B. Póczos, and A. Smola, “Stochastic variance reduction for nonconvex optimization,” in *International Conference on Machine Learning*, 2016, pp. 314–323.
- [63] H. Zhang and S. Sra, “Towards Riemannian accelerated gradient methods,” *arXiv preprint arXiv:1806.02812*, 2018.
- [64] G. Becigneul and O.-E. Ganea, “Riemannian adaptive optimization methods,” in *International Conference on Learning Representations*, 2019. [Online]. Available: <https://openreview.net/forum?id=r1eiqi09K7>
- [65] D. P. Kingma and J. Ba, “Adam: A method for stochastic optimization,” *arXiv preprint arXiv:1412.6980*, 2014.
- [66] S. Dasgupta, “Learning mixtures of gaussians,” in *40th Annual Symposium on Foundations of Computer Science*. IEEE, 1999, pp. 634–644.
- [67] P. Arbelaez, M. Maire, C. Fowlkes, and J. Malik, “Contour detection and hierarchical image segmentation,” *IEEE Trans. Pattern Anal. Mach. Intell.*, vol. 33, no. 5, pp. 898–916, May 2011. [Online]. Available: <http://dx.doi.org/10.1109/TPAMI.2010.161>
- [68] Z. Wang, A. C. Bovik, H. R. Sheikh, E. P. Simoncelli *et al.*, “Image quality assessment: from error visibility to structural similarity,” *IEEE Transactions on Image Processing*, vol. 13, no. 4, pp. 600–612, 2004.